ELSEVIER

Marine Geology 181 (2002) 195–213

MARINE GEOLOGY
INTERNATIONAL JOURNAL OF MARINE GEOLOGY, GEOCHEMISTRY AND GEOPHYSICS

www.elsevier.com/locate/margeo

Flow and sediment suspension events on the inner shelf of central California

C.D. Storlazzi *, B.E. Jaffe

Coastal Geology and Imaging Laboratory, United States Geological Survey, Pacific Science Center, University of California, 1156 High Street, Santa Cruz, CA 95064-1077, USA

Received 26 January 2001; accepted 16 July 2001

Abstract

The US Geological Survey conducted a field experiment in the late spring and early summer of 1998 off northern Santa Cruz County, California, to study sediment fluxes along the central California shelf. As part of this study, a bottom-mounted instrument package was deployed in a sediment-filled paleo-stream channel ($h = 12$ m) off a pocket beach to measure waves, currents, suspended-sediment concentration, temperature, salinity, and seabed-level changes. The observations of suspended-sediment concentration revealed intermittent, intense periods of sediment suspension near the bed that were associated with the passage of individual large waves or wave groups. We used an ensemble averaging technique to characterize the temporal structure of near-bed sediment suspension events (SSEs) defined as when the near-bed instantaneous concentration exceeded the mean by three standard deviations. During the 800 h of deployment, over 9500 SSEs occurred. The 3917 SSEs that began under onshore flow were found to have a different temporal structure than the 5650 events that began during offshore flow. The longer mean duration of the onshore flow events caused an average of 83% of the sediment suspended during the course of the events to be carried offshore after the reversal of flow. All of the sediment suspended during the offshore events was carried offshore due to the shorter mean duration of these events. SSEs are shown to contribute 12% on average and up to 95% of the total sediment suspended by mass, demonstrating the importance of these events to sediment transport in this type of environment. Suspended-sediment transport models developed for the shelf, which use the product of the mean current and the mean suspended-sediment concentration, cannot accurately model the magnitude and direction of suspended-sediment transport on this energetic inner shelf due to the lack of information regarding the instantaneous coupling between fluid flow and sediment suspension. We conclude that time-variant models must be used to accurately model suspended-sediment transport in this type of environment.

Keywords: Rocky coastline; Waves; Currents; Sediment suspension event; Suspended; Sediment transport; Inner continental shelf

1. Introduction

The inner continental shelf serves as the transition zone between the surf zone and the rest of the continental shelf. Exchanges of sediment between the inshore and offshore regions influence the morphologies and sediment budgets of both

* Corresponding author. Tel.: +1-831-459-2403; Fax: +1-831-459-3074.

E-mail addresses: manta@earthsci.ucsc.edu (C.D. Storlazzi), bjaffe@usgs.gov (B.E. Jaffe).

0025-3227/02/$ – see front matter
PII: S0025-3227(01)00267-5

regions. In order to understand the consequent sedimentary characteristics, we need to define both the direction and magnitude of the exchange processes. Mesoscale motions dominate the hydrodynamics over the continental shelf. The inner continental shelf provides an effective coastal boundary to these mesoscale flows (i.e. Csanady, 1982) and wave energy is dissipated by bottom friction. Gravity waves interact with quasi-steady currents such as tidal currents, wind-driven upwelling and downwelling (Niedoroda et al., 1984; Wright et al., 1986), lower frequency flows of amplitude modulated waves (Shi and Larsen, 1984) and gravity-driven motions (Seymour, 1986). In addition to the hydrodynamic factors, further complications arise in determining the magnitude of transport from sedimentary characteristics and bedforms (Vincent et al., 1991; Hay and Bowen, 1994; Gallagher et al., 1996). The quantification of the process thus requires an understanding of both sediment dynamics and hydrodynamics (i.e. Wright, 1987).

Approximately 500 km (28%) of California's coast, and much of the remaining Pacific Ocean coast as well, is characterized by uplifted, rocky shorelines along tectonically active margins. The morphology of these shorelines includes coastal mountains, seacliffs, and small pocket beaches at stream mouths. The near-shore and innermost shelf off central and northern California are sparsely covered with sediment, with bedrock commonly exposed on the shoreface (Cacchione et al., 1984, 1987; Tait et al., 1992; Tait, 1995; Anima, 2000). Bathymetric variations commonly mirror the onshore topography. Headlands typically extend offshore as barren, bathymetric highs and pocket beaches or coastal stream valleys are fronted by more gently sloping bathymetric depressions. The studies by Anima and Tait also have shown that substantial volumes of sand-sized sediment are stored in these depressions at shallower depths, whereas finer sediment commonly is observed farther offshore. Tait (1995) and Storlazzi and Field (2000) observed relief on the order of 0.1–10 m between these rocky highs and adjacent sediment-filled basins along the central coast of California. Headlands and submerged bedrock ridges can steer currents and form barriers to the alongshore transport of sediment in a manner not commonly observed along coastal plain-bound shorelines. Although this type of coast, reflecting areas of tectonic uplift and glaciostatic rebound, is common worldwide, there is little documentation of hydrodynamics and sediment suspension processes on the shoreface in this type of environment.

An extensive, multi-year field study was conducted by the US Geological Survey to understand the geology, geomorphology, and oceanography in the Monterey Bay National Marine Sanctuary. As part of this study, four separate instrument packages were deployed in a line across the shelf of central California in 1998 as part of the Monterey Bay Sediment Exchange Experiment (MOBSEE) to study the sediment fluxes along the central coast of California and into Monterey Bay. Moorings, located on the relatively planer mid- and outer shelf at depths of 30, 70 and 120 m, comprised the seaward part of the line; the findings from these instruments are discussed by Xu et al. (2002). A robust, bottom-mounted instrument package was deployed on the inner shelf at a depth of 12 m on the landward edge of this line in a sediment-filled bathymetric depression bounded by rock outcrops off a pocket beach. The goal of the research reported here is to improve understanding of the nature of fluid flow and sediment fluxes on a rocky, high-energy shoreface using the data from this inner shelf station.

2. Field experiment

2.1. Site description

These field observations and results were obtained from instruments deployed along the central portion of the Monterey Bay National Marine Sanctuary off northern Santa Cruz County, California (Fig. 1). The central coast of California is an active continental margin experiencing uplift anywhere from 0.2–1.6 mm/yr (Page et al., 1998). The shoreline is incised with a flight of marine terraces and seacliffs 3–30 m high that are composed of Tertiary sedimentary rocks, primarily

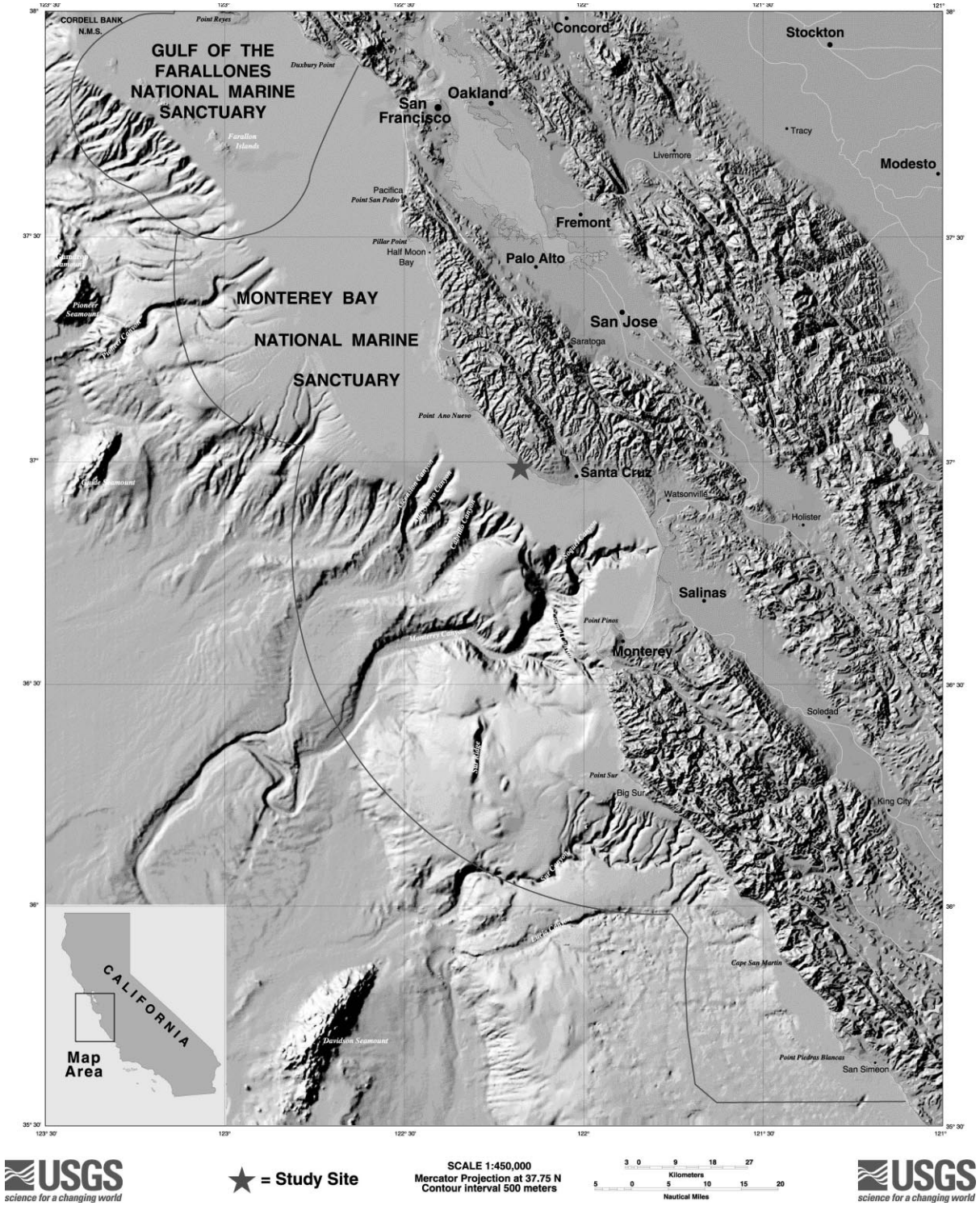

Fig. 1. The experiment site is located approximately 15 km north of Santa Cruz. This stretch of coast is outside of Monterey Bay and exposed to high wave energy, typically from the northwest.

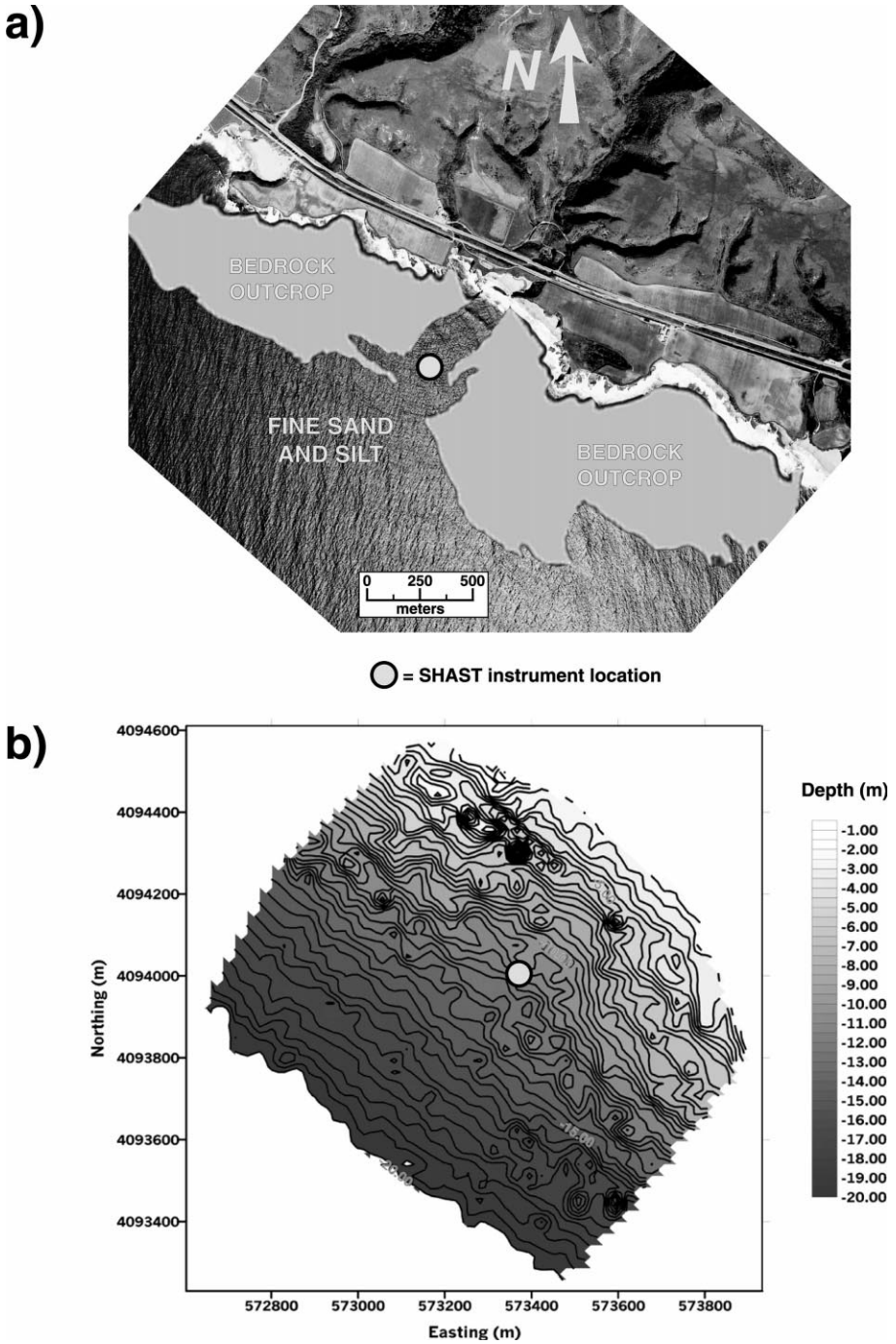

mudstone and lesser amounts of sandstone (US Army Corps of Engineers, 1985).

Yellow Bank Beach is an approximately 100-m-long pocket beach located 2.4 km southeast of Davenport, in northern Santa Cruz County. This beach is bounded by headlands that extend beyond the low-energy surf zone. The headlands extend offshore as rocky bathymetric highs, and

Fig. 2. Morphology of Yellow Bank Beach. (a) Aerial photograph of the study area overlain by a mosaic of interpreted bottom type from a sidescan sonar survey by Anima (2000). The instrument package was located in a paleo-stream channel flanked by rock outcrops. The coastline is irregular with headlands bounding pocket beaches. Note the correlation between streams that incised the marine terraces and the sediment-filled channels on the upper shoreface. (b) The bathymetry in the study area. The data shown here are the result of over 40 km of high-resolution shore-normal and shore-parallel survey lines collected using the HYPAC navigational package and real-time kinematic differential global positioning system. In combination, these methods provided depth and position information at a >3-cm resolution even when the survey vessel was traveling at 20 km/h. This mosaic was compiled from over 66 000 individual data points.

the pocket beaches are fronted by more gently sloping bathymetric depressions, as shown in Fig. 2. This instrument package was deployed roughly 470 m offshore Yellow Bank Beach in 12 m of water. The instrument was located in a sediment-filled depression that is interpreted to be a paleo-stream channel incised during periods of lower sea level (Anima, 2000). There is substantial relief (>2.0 m) between rock outcrops and the floor of the sediment-filled depression.

Divers collected surficial bottom sediment from underneath the instrument during the deployment and recovery of the instrument package. The upper few centimeters of sediment is unimodal and well sorted, with a mean grain size (D_{50}) of 0.13 mm (fine to very fine sand); the mode, representing 75% of the surficial bed size distribution, was between 0.10 and 0.25 mm. Small ($\eta_r = 0.01$–0.03 m, $\lambda_r = 0.1$–0.2 m) ephemeral anorbital sand ripples covered the bed and dense aggradations of dendrasters (sand dollars) were observed near the instrument during both deployment and recovery.

The waves that approach the study area are characterized by three dominant modes. The northern hemisphere swell is typically generated by cyclones in the north Pacific and in the Gulf of Alaska during the winter months (November–March); this swell can attain deep-water wave heights exceeding 8 m. The southern hemisphere swell is generated by storms off of New Zealand, Micronesia, or Central America during summer months. Although these storms generally produce smaller waves than the northern hemisphere swell, the southern hemisphere swell often has very long periods (>20 s). Local wind-driven seas typically develop rapidly when low pressure systems pass near central California in the winter months or when strong sea breezes are generated during the spring and summer (National Marine Consultants, 1960; Meteorology International, 1977). The winds typically come from the northwest during the summer months due to a region of high pressure commonly lying offshore of central California. During the winter, the winds typically take on a more westerly to southwesterly direction as a region of low pressure develops over the Gulf of Alaska that drives storms across northern and central California (Strub et al., 1987).

2.2. Instrumentation

The shoreface hydrodynamic and sediment transport (SHAST) instrument package was configured to collect hydrodynamic and sediment measurements in the benthic boundary layer (Fig. 3). The sensors were mounted in a cantilever fashion off a 1.25-m-long pipe that was emplaced by divers at the study site. This structure was bolted onto a 3.3-m-long vertical stainless steel pipe jetted over 1 m into the seafloor, allowing the sensors to be arranged at varying heights above the bed. A Marsh–McBirney model 512

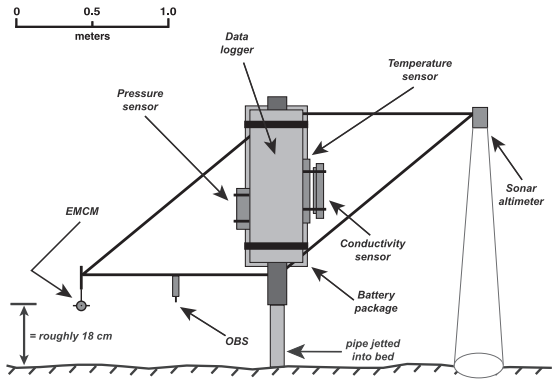

Fig. 3. Design of the SHAST instrument package showing the relative location of the sensors, data logger, and battery package.

bi-axial electromagnetic current meter (EMCM) was initially deployed 0.18 m above the bed and mounted vertically to measure two orthogonal components of horizontal flow. Also mounted at roughly the same elevation above the bed (0.32 m horizontally from the EMCM) was a D&A Instruments model 3 optical backscatter sensor (OBS) to measure suspended-sediment concentrations.

Since intensity of the backscattered signal is a function of grain size, the OBS was calibrated by D&A Instruments for the range of 0–20 g/l with a bulk surficial sediment sample collected at the site. While this method would overestimate the suspended-sediment concentration if the fines were preferentially suspended, the narrow grain-size distribution and very low ($<7\%$) mud content made us confident in our calculations of suspended-sediment concentration. A Paroscientific model 8DP060-1 digiquartz pressure sensor was mounted initially 0.46 m above the bed. A downward-facing Konsberg Simrad Mesotech Systems model 807 analog sonar altimeter initially mounted 0.82 m above the bed provided a time series of changes in bed elevation. A Seabird Electronics model 3S temperature sensor and Seabird Electronics model 4M conductivity sensor were also mounted on the instrument package to measure water properties and define periods of upwelling or downwelling. The pressure sensor, OBS, and EMCM collected 2048 samples at 2 Hz (17.1 min of data per burst) at the beginning of each hour while temperature, conductivity, and altimeter data were collected for 30 s at 2 Hz (60 samples per burst) every hour.

The SHAST instrument package was deployed for a total of 1534 h from May 6th, 1998 through July 9th, 1998. Due to hardware problems, however, the power drain by the sonar altimeter on the system made the measurements collected after the first half of the deployment unreliable. The variation in bed elevation observed while the altimeter functioned properly were quite small (maximum = 3 cm, mean <1 cm) and were likely due to the presence of anorbital ripples as discussed previously. Even though concentration decays exponentially with elevation above the bed and the phase relationship between concentration and velocity is sensitive to the measurement position, we feel that the bed changes would not substantially affect our calculations on suspended-sediment concentration. This is due not only to the small size of the ripples, but also their likely absence during the more energetic periods when the concentrations are high due to the transition into upper plane bed conditions as modeled by Storlazzi (2000). We therefore report only the 33 days (800 h) of data at 24 bursts per day from the OBS, EMCM, pressure, temperature, and conductivity sensors. Surface wind, atmospheric pressure, and precipitation data were collected by a meteorologic station on top of the University of Santa Cruz (UCSC) Long Marine Laboratory roughly 9 km to the southeast of the study site. Directional wave data collected by a deep-water ($h \sim 540$ m) offshore buoy (CDIP #02901) located about 140 km northwest of the field area were used, in conjunction with the meteorologic data, to constrain the external meteorologic and wave forcing on the system.

3. Methods

We evaluated the wave spectrum using an ensemble and band-averaging power autospectrum. This routine applied a 256-s Hanning window with 50% overlap and a linear de-trend to replace the truncated degrees of freedom and hence increase the reliability of the results. The dominant wave period (T_p) was determined after spectrally correcting the spectrum for pressure attenuation with depth using linear wave theory using a high-frequency cut-off of 0.33 Hz. The significant wave height (H_s) was calculated spectrally using the Birkemeier et al., (1989) method and a bandwidth of 0.33–0.04 Hz (3–25 s). Wave direction was computed from cross-shore (u) and alongshore (v) current flows using the Madsen (1994) centroid averaging binned variance method. A lower limit of 33% of the maximum variance was set as the cut-off for determining the centroid of the variance peaks. We utilized 1° directional bins. In order to determine the distance to the bed from the sonar altimeter, the two-tiered bin 'seabed-finding' algorithm of Gallagher et al. (1996) with

a 1.0-mm resolution was applied to the observed time series during each burst. The OBS signal was 'de-spiked' by removing all instantaneous jumps in the concentration time series that exceeded the mean concentration for the burst plus three times the standard deviation for the burst and that had a width of only one time step (0.5 s).

Suspended-sediment fluxes were calculated using the Madsen (1994) spectral wave–current bottom boundary layer model that incorporates the non-linear interaction between waves and currents to estimate a depth-integral of the flux profile from a single-point velocity measurement. The hydrodynamic part of the model uses a cubic eddy viscosity profile (Signell, 1989; Signell et al., 1996) with an inflection at the top of the wave–current boundary layer and assumes no Coriolis forcing, which is valid for this shallow depth. The model was run using six grain-size classes from 1.5–4.0ϕ (0.35–0.06 mm) with 0.5ϕ increments to calculate the suspended-sediment profiles.

Due to the aperiodic nature of sediment suspension observed during deployment and preliminary examination of the data, we chose to focus our analysis of the concentration time series in an event-by-event nature by defining periods of intense suspension. Sediment suspension events (SSEs) were defined based on the statistical properties of the concentration distribution, following Jaffe and Sallenger (1992), as summarized here. As in the surf zone, the distribution of concentration measurements on the inner shelf was skewed, with many low values and fewer high values. Although many different thresholds could be used to define 'events', we chose to define events as when the instantaneous concentration (C) exceeded the mean concentration ($\overline{C}$) by three standard deviations and had a duration greater than one sample (0.5 s). More than 95% of events we evaluated had durations greater than four samples (2.0 s). This threshold selects only the most statistically significant events. In order to define event durations and mean event concentration, the event start/end threshold was chosen to be $\overline{C}$ (Fig. 4). SSE characteristics and temporal structure were evaluated using an automated algorithm. These SSEs were distinguished by either shoreward or seaward peaks in the cross-shore sediment flux, estimated by the product UC, following the methods of Jaffe and Sallenger (1992) and Dick et al. (1994). This product was used merely as a means of determining the direction

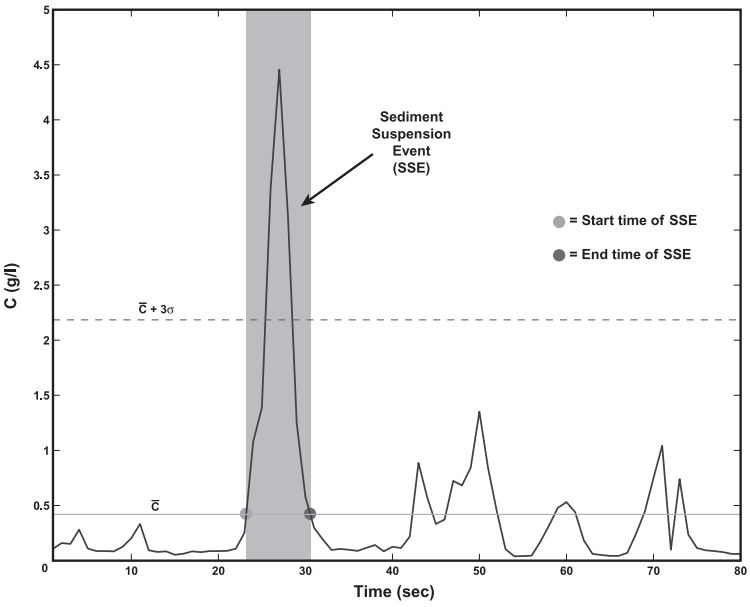

Fig. 4. Example time series of suspended-sediment concentration showing the parameters used to define suspension events.

of the cross-shore transport during each event, in order to discriminate between those events that contributed to onshore sediment transport from those leading to seaward sediment transport. Suspension events were identified by the following criteria: if an event (when $C \geq \overline{C}+3\sigma$) started during a period of onshore (offshore) flow, it was considered to be an onshore (offshore) suspension event.

4. Results and discussion

4.1. Physical forcing

The SHAST instrument package was deployed through the late spring and early summer of 1998. A series of moderate storms struck the central coast of California. The two most intense storms occurred during May 12–13th and May 27–29th. Deep-water wave heights exceeded 3 m during the deployment, and the dominant deep-water wave periods were typically 10–15 s during storms (Fig. 5). Sea-level barometric pressure dropped below 1000 and 1005 mbar during the two largest storms. The winds during the spring are typically shore-parallel to the southeast, driving the strong upwelling common to the open coast of central California (Strub et al., 1987). Pronounced changes in the wind direction were observed during the two largest storms; the May 12–13th and the May 27–29th storms were characterized by 8 and 12 m/s, respectively, sustained winds toward the north (Fig. 5).

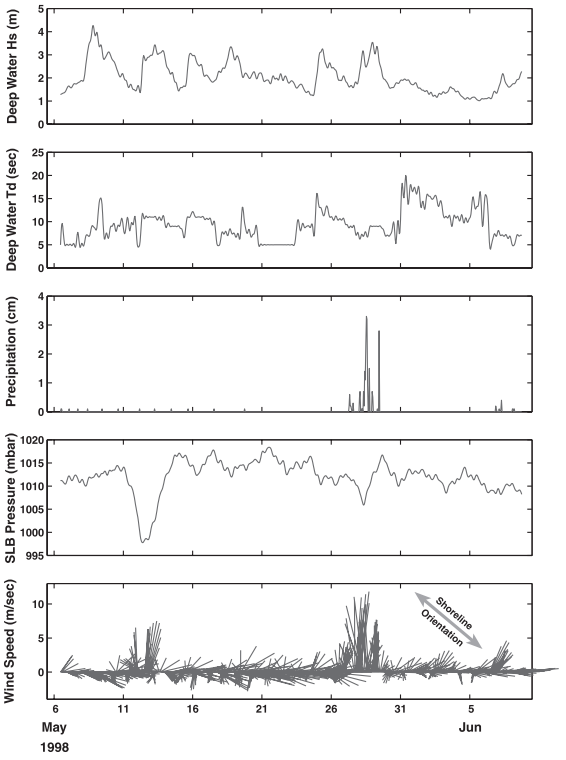

Fig. 5. Meteorology and oceanography for the period of deployment. Deep-water significant wave heights and dominant periods are from the CDIP Point Reyes buoy (#02901). Precipitation, sea-level barometric pressure, and wind speed and direction are from the UCSC Long Marine Laboratory meteorologic station. All vectors are projected geographically (north = up, east = right).

4.2. Tides, waves and physical properties

The tides at the study site are characterized as a mixed type; the pressure time series displays both diurnal and semi-diurnal tidal signals (Fig. 6). The maximum spring tide range during the deployment was approximately 2.5 m, and the diurnal and mean tidal ranges were roughly 1.5 and 1.0 m, respectively. Waves at the study site were on the order of 2 m during the largest storms, displaying a significant energy loss to refraction and bottom dissipation between the deep-water CDIP buoy (Fig. 5) and at the SHAST package (Fig. 6). In general, high mean suspended-sediment concentrations near the bed were observed during the periods of high wave energy ($R^2 = 0.0679$, significant at the 0.1% level for $n = 800$). The temperature and salinity time series display not only daily fluctuations related to internal tides but also longer-period fluctuations resulting from the passage of storms. The transitions from periods of relatively cold, high-salinity conditions to warm, low-salinity conditions near the bed observed on May 12th and May 27th are due to the passage of the two largest storms discussed earlier. These storms, which had strong sustained winds to the north, drove warm surface water onshore through Coriolis forcing and shut down the upwelling that is typically observed in late spring and summer.

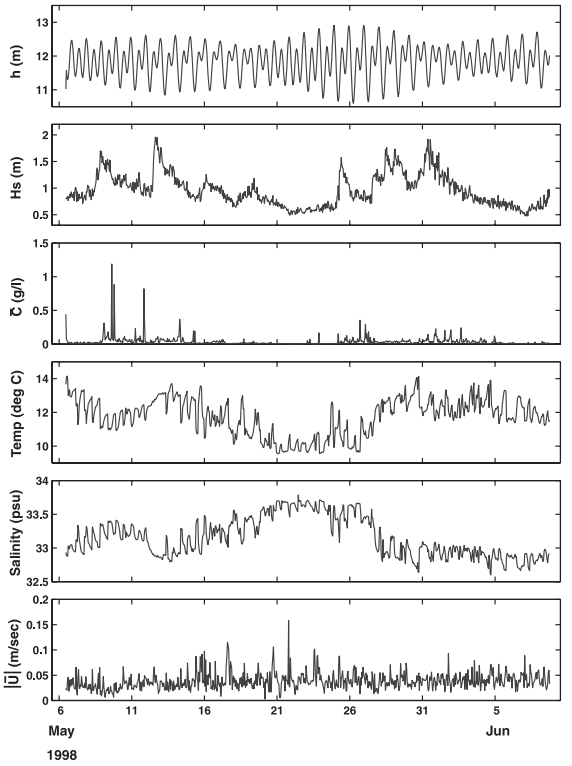

Fig. 6. Time series of burst-averaged water depth (h), significant wave height (H_s), suspended-sediment concentration (C), temperature, salinity, and current speed (U) for the entire deployment. The deployment covered two complete tidal cycles. Note the correlation between significant wave height and mean concentration. Also apparent are the daily fluctuations in temperature and salinity that are related to strong afternoon sea breezes from the northwest that intensify local upwelling.

4.3. Currents

The mean of the burst-averaged currents during the deployment were approximately 3 cm/s, which is near the resolution limit of the Marsh–McBirney EMCM. These flows are assumed to be primarily long-wave- and wind-driven. A full tidal harmonic analysis (Foreman and Henry, 1979) demonstrated that only 23% of the total variance in the mean current's record could be explained by 35 tidal constituents. The first five constituents, in decreasing contribution to the mean flow, were: K1 (lunar–solar diurnal), MM (lunar monthly), M1 (lunar diurnal), O1 (main lunar diurnal), and MSF (lunar–solar fortnightly). Due to the low variability explained by the harmonic analysis, we preformed simple bandpass filtering to evaluate the relative contributions of different components to the near-bed currents. We assumed the semi-diurnal and diurnal tidal components to be equivalent to the time-series output from the harmonic analysis bandpass filtered at 10–16 and 20–28 h, respectively, as proposed by Wright et al. (1999). Supratidal currents were 3–10-h bandpass-filtered, while the subtidal currents were 36-h low-pass-filtered following Wright et al. (1999). The mean with 95% confidence intervals and maximum speeds contributed by each component during the deployment are summarized in Table 1. The mean current for the entire period of the deployment is directed offshore and to the southeast. The subtidal and supratidal currents were generally three to five times as strong as the tidal components. Wave orbital motions, which were 3–30-s bandpass-filtered in the individual burst time series, dominated the near-bed flow with speeds that were at least an order of magnitude greater than the wind-driven and tidal currents. Infragravity wave motions, which were 30–300-s bandpass-filtered in the individual burst time series, were generally 150–200% of the wind-driven currents magnitude; the maximum infragravity motions, however, exceeded 0.06 m/s dur-

Table 1
Magnitudes of near-bed flow components from the EMCM roughly 18 cm above the bed

Components (cm/s)	Mean ± 2σ	Maximum
Cross-shore wave orbital motions	10.5 ± 3.3	117.8
Cross-shore infragravity wave motions	1.7 ± 1.1	6.8
Cross-shore supratidal currents	1.1 ± 1.9	6.2
Cross-shore subtidal currents	0.8 ± 1.5	6.4
Semi-diurnal tidal currents	0.2 ± 0.3	0.6
Diurnal tidal currents	0.3 ± 0.8	1.7

ing some of the periods dominated by swell with high groupiness.

4.4. Sediment suspension

Time-series plots of sea surface elevation and suspended-sediment concentration near the bed are shown in Fig. 7 for a burst during environmental conditions typical for this time of year (hour 77 of the deployment; May 8 at 15.00 h). Sediment suspension occurred as intermittent events at time scales near that of the incident wave period as displayed by the water depth (h) and C time series. Large low-frequency modulation related to the passage of wave groups (Hanes, 1991; List, 1991) is also apparent. The suspended-sediment concentration from 200–400 s in this burst appears to correlate very well with the passage of a large, narrow-banded wave group. Fig. 8 shows that intense sediment suspension during this time period (second 200–400 in burst 77) often occurs at half the dominant incident wave period, which had been commonly ob-

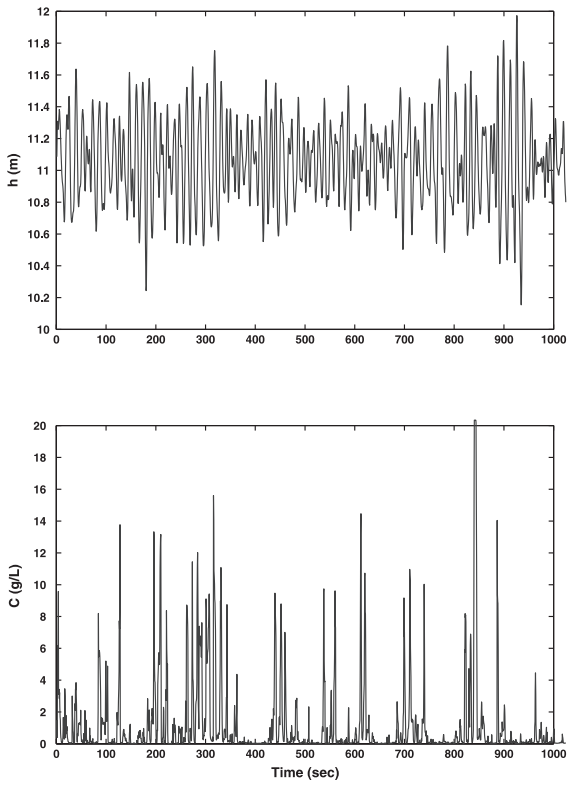

Fig. 7. Example burst time series of water depth and suspended-sediment concentration at 18 cmab (cm above the bed) during hour 77 of the deployment ($H_s = 1.2$ m, $T_p = 12.8$ s) displaying wave groups and the large number of suspension events > 5 g/l at this water depth. Note the correlation between suspended-sediment concentration and incident waves and wave groups during this burst, which is characterized by typical environmental conditions for this time of year. The correlation between water depth and suspended-sediment concentration during this burst is significant above the 1% level.

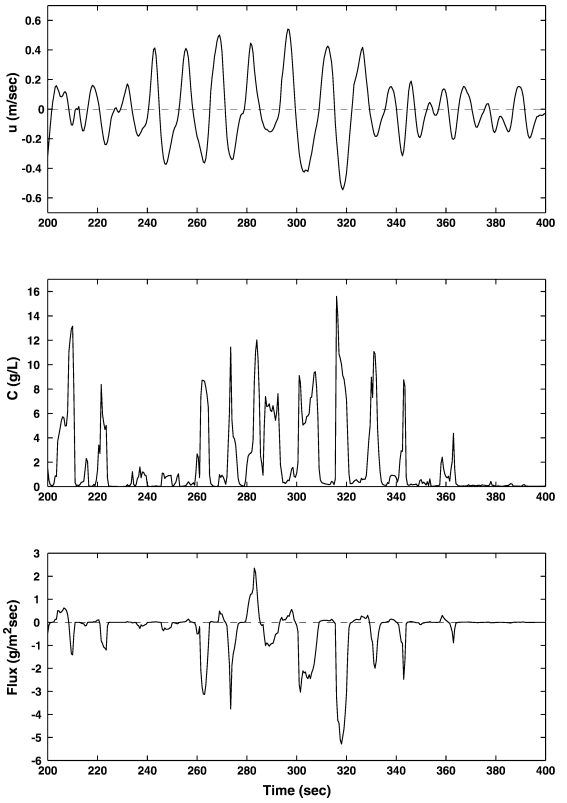

Fig. 8. The cross-shore current velocity (positive = onshore) and suspended-sediment concentration at 18 cmab for the period from 200–400 s during hour 77 of the deployment (see Fig. 7). The suspended-sediment concentration is shown to often occur not only at half the dominant incident wave period, but also at roughly the same frequency as the incident waves. This lower frequency of sediment suspension suggests that a specific direction of orbital wave motion may more effective at suspending sediment high in the water column, which may be due to the orientations of the mean current, waves, and bedforms relative to one another.

served in and near the surfzone (Hanes and Huntley, 1986; Osborne and Greenwood, 1992; Hay and Bowen, 1994). Many times, however, sediment was suspended at roughly the same frequency as the incident waves, rather than at half the incident wave frequency, similar to the observations made on the inner shelf by Wright et al. (1991) and just outside the surfzone by Dick et al. (1994). This finding suggests that a specific direction of orbital wave motion may be more effective at suspending sediment high in the water, as shown in the bottom panel of Fig. 8. This could result from high shear at the top of the wave–current boundary layer due to an opposing current or asymmetric bedforms that would cause differences in the intensity and elevation of vortexes being shed from the bed. Overall, this data further supports the importance of waves in suspending sediment on the Californian shelf, as found by Cacchione and Drake (1982), Sherwood et al. (1994), Ogston and Sternberg (1999).

The maximum correlation between U and C (Fig. 9a,b) for all of the bursts during the deployment occurs at +1 s lag, indicating that on average, the suspended-sediment concentration peaks 1 s before the cross-shore current velocity reaches its maximum. We infer from this +1 s lag that the initial suspension is not being driven by the shear stresses imposed on the bed when the near-bed flow reaches its maximum. Even assuming near-bed laminar flow where the shear stress leads the velocity by 45°, which is unlikely due to the bed roughness and the nature of near-bed flow in the presence of waves and currents, the +1 s lag would imply the instantaneous advection of the sediment from the bed to the elevation of the OBS ($\sim$0.2 m). This conclusion that the initial sediment entrainment is driven by something oth-

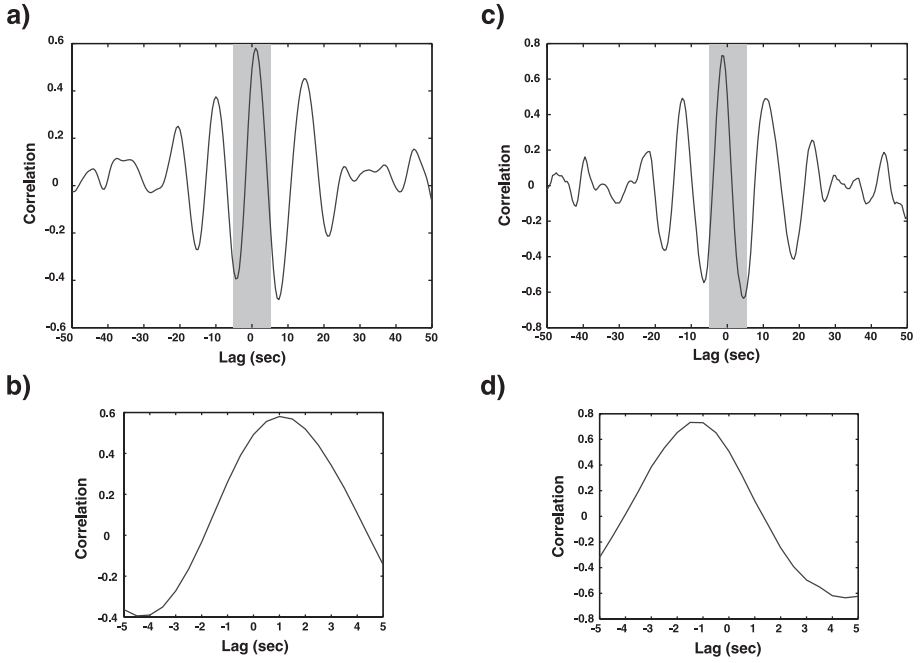

Fig. 9. Cross-correlation between suspended-sediment concentration and flow. (a) Cross-shore current velocity and suspended-sediment concentration at 18 cmab with a ±50 s maximum lag. (b) Cross-shore current velocity and suspended-sediment concentration with a ±5 s maximum lag. The maximum correlation is at +1.0 s lag. On average, the suspended-sediment concentration peaks 1.0 s before the cross-shore current velocity reaches its maximum. (c) Cross-shore current acceleration and suspended-sediment concentration at 18 cmab with a ±50 s maximum lag. (d) Cross-shore current acceleration and suspended-sediment concentration with a ±5 s maximum lag. The maximum correlation is at −1.0 s lag. On average, the suspended-sediment concentration peaks 1.0 s after the cross-shore current acceleration reaches its maximum.

er than the peak shear stress is further reinforced by the fact that, on average, the suspended-sediment concentration peaks 1 s after the cross-shore current acceleration reaches its maximum. This is demonstrated by the maximum correlation between the cross-shore acceleration (Au) and C at a -1 s lag (Fig. 9c,d). This suggests that it is the rapid decay, reversal, and growth of the wave boundary layer in its acceleration that initially entrains sediment. This theory is supported by divers' observations. This sediment then reaches the elevation of the OBS on average 1 s later due to 'pumping' by the high shear both near the bed and at the top of the wave–current boundary layer, a lag similar in duration as those observed by Huntley and Hanes (1987) and Foster (1997). These consistent phase relationships also imply that non-random processes are driving the sediment suspension. A random process such as sediment clouds generated at varying locations advecting past the sensor would not result in a consistent phase relationship. The intermittent nature of this suspension led to the examination of the data by way of defined suspension events.

4.5. Temporal structure of sediment suspension events

During the first 800 h of the deployment, we identified 9567 significant SSEs in the near-bed suspended-sediment concentration, with 3917 onshore events and 5650 offshore events. Although the concentration and duration of the events varied significantly from event to event, the general characteristics of the onshore and offshore events could be compared by ensemble averaging. We explored the temporal structure of the suspension events by ensemble-averaging the events. We aligned the start of each event (when $C \geq \overline{C}$) and then averaged the events over the period from 5 s before to 15 s after the start of the event (Fig. 10).

Prior to the onshore suspension events, the suspended-sediment concentration 0.18 m above the bed is fairly steady and low, approximately 0.05 g/l. The cross-shore flow peaks onshore, at approximately 0.12 m/s. Within 0.5 to 1.0 s after the onshore velocity peaks, the suspended-sediment concentration begins to increase rapidly by almost a factor of five. Within a second after the initiation of the event, the concentration peaks at 0.24 g/l on average. A half-second later, the cross-shore velocity reverses to offshore flow and peaks approximately 2.0 s later. Following the peak of the suspension event, the sediment concentration decreases relatively slowly, taking almost 5.0 s (half the average wave period) before attaining pre-event concentrations. A consequence of this long duration, during which flow reverses, is that much of the 0.0305 g/cm^2 s shoreward flux during onshore flow appears to be offset by the

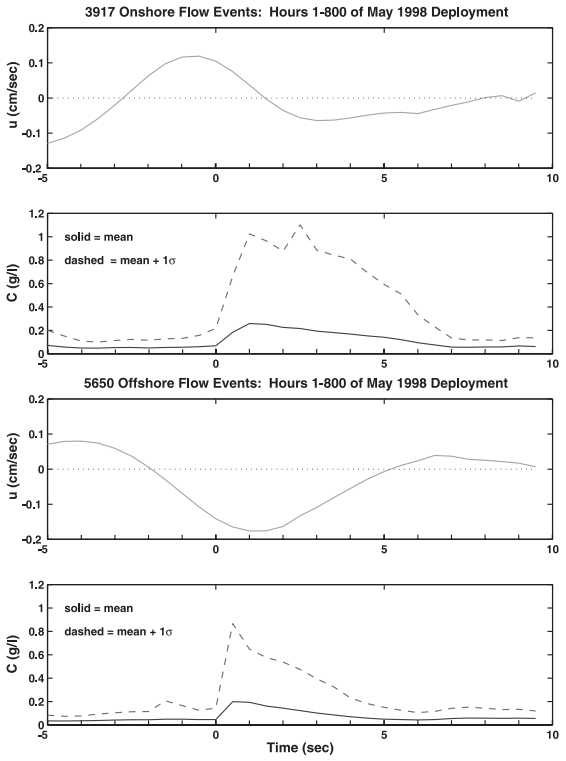

Fig. 10. Ensemble-averaged concentration and cross-shore current velocities for 3971 onshore events and 5650 offshore events in the cross-shore flux at 18 cmab. The solid lines in the concentration time series are ensemble means while the dotted lines are the means plus one standard deviation. Note the longer mean duration of the onshore suspension events. The flow typically reverses, driving some of the suspended sediment offshore. This is in contrast to the shorter duration offshore events, which do not last long enough for flow to reverse and therefore cause a reversal in transport.

0.0830 g/cm^2 s offshore flux after the flow reversal before settling, contributing to a net ensemble-averaged offshore flux of 0.0525 g/cm^2 s.

The ensemble-averaged offshore flow events differ in several ways. The suspended-sediment concentration, roughly 0.04 g/l, is slightly lower before the onset of the event. The reversal to offshore flow typically occurs 2.0 s before the initiation of the suspension event and peaks approximately 1.5 s after the start of the event. The concentration rapidly increases from the pre-event levels, peaking roughly 0.5 s after the start of the event, 0.5 s quicker on average than during the onshore events. Concentration also increases by a factor of five to 0.20 g/l, slightly lower than during onshore events. The offshore flow typically peaks 1.0 s after the beginning of the event, just at the time when the concentration starts to drop off. The suspended-sediment concentration re-attains pre-event levels much more rapidly than in the onshore events, approximately 4.0 s after the beginning of the event and 3.5 s on average after the concentration peaks. As flow reverses 5.0 s on average after the initiation of the event, all 0.1990 g/cm^2 s of the ensemble-averaged suspended-sediment flux is driven offshore.

The asymmetric form of the onshore flux events is similar to those observed in the surf zone (Jaffe and Sallenger, 1992) and in shallow ($\sim$2 m) water just outside the surf zone (Dick et al., 1994). The asymmetry of the offshore flux events discussed here differs from the symmetry of those observed by Dick et al. (1994), who theorized that the symmetry of the SSEs was caused by resuspension of sediment settling from a previous onshore flux event. They concluded this from the observation that the concentration began to increase at the time of maximum onshore flow, and peaked at the time of the maximum offshore flow. Here, however, the offshore events clearly both start and peak under offshore flow, and are therefore likely not the result of resuspension of settling sediment. While vortex formation and ejection from the lee of bedforms could cause problems when interpreting these suspension events, we do not feel that this is significant in the case of our results due to: (a) the small size of the observed and modeled ripples, and (b) their likely absence during periods of high suspension as modeled by Storlazzi (2000).

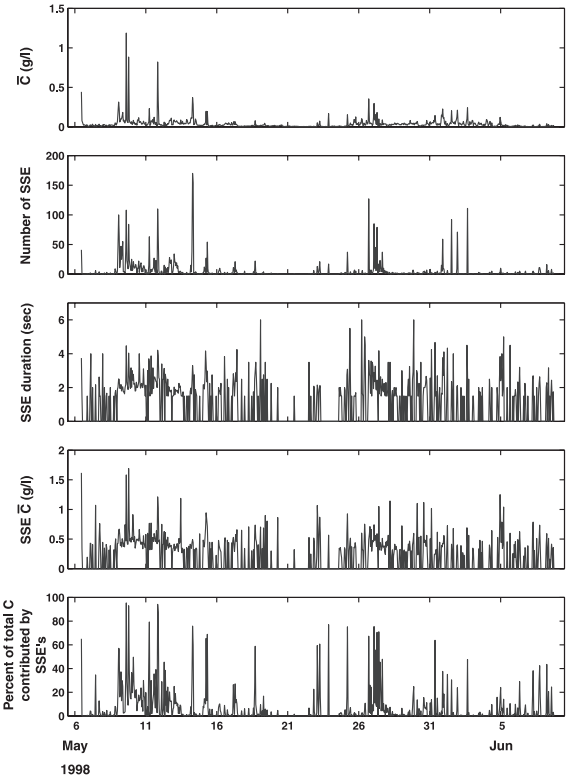

Fig. 11. Burst-averaged mean concentration, the number of suspended-sediment events, the mean event duration, the mean event concentration, and the percent of total suspended sediment contributed by suspended-sediment events during the deployment. Note that all of the parameters increase with increased wave energy, demonstrating the episodic nature of suspended-sediment transport in this type of environment.

4.6. Sediment suspension event characteristics

The character of SSEs is shown in Fig. 11, and their statistics are displayed in Table 2. The number of SSEs per burst is well correlated with the mean concentration, significant wave height, and wave orbital velocity. For the entire period when data was collected, there was on average one SSE every 85.8 s (1.43 min). The mean duration of events is just over 1.5 s. During more energetic periods (i.e. May 9th through May 12th), the

Table 2
SSE statistics roughly 18 cm above the bed

	Entire record		$U_{rms} \geq 0.3$ m/s
	mean ± 2σ	maximum	mean ± 2σ
Number of SSEs	10.2 ± 42.1	170	17.2 ± 41.8
SSE duration (s)	1.7 ± 1.9	12.0	2.3 ± 1.7
SSE mean concentration (g/l)	0.34 ± 0.56	1.69	0.47 ± 0.43
Percent of total burst concentration contributed by SSEs (%)	12.5 ± 28.4	95.3	14.6 ± 32.2

mean duration increases to more than 2 s. These durations are much shorter than 5–7-s SSEs observed in the surf zone (Jaffe and Sallenger, 1992). While the mean concentration during the SSEs is only 0.34 g/l, the maximum instantaneous concentration during the bursts often exceeds 20 g/l, the maximum setting of the OBS for the deployment. When the near-bed horizontal orbital velocities are high (>0.3 m/s), the ensemble-averaged mean concentration is over almost 40% greater than concentrations computed for all the SSEs. Even though the mean concentrations are low and their durations are relatively short, the SSEs contribute on average 12.5% of the total suspended sediment observed and up to 95% during energetic periods. During this deployment when only a few moderate storms struck the study area, the SSEs contributed less than 30% of the total suspended sediment observed during 731 of the 800 total bursts (91% of the deployment). Thus, these short-duration, high-concentration events appear to make a substantial contribution to suspended-sediment transport on the inner shelf, and likely contribute even higher percentages to the total suspended sediment during very energetic periods.

4.7. Forcing and the direction of sediment transport

The dominant wave direction measured at the study site was to the southeast (Fig. 12). During the major storms, however, the waves approached from a more westerly direction. The wind directions were in general similar to the waves, typically to the southeast, except during the storms when the winds took on more northerly directions. Although the wind and waves were generally directed to the southeast, the mean currents were primarily directed to the southwest, roughly 90° from the direction of the waves and winds, and almost perpendicular to the shoreline. These near-bed currents were often oriented the opposite

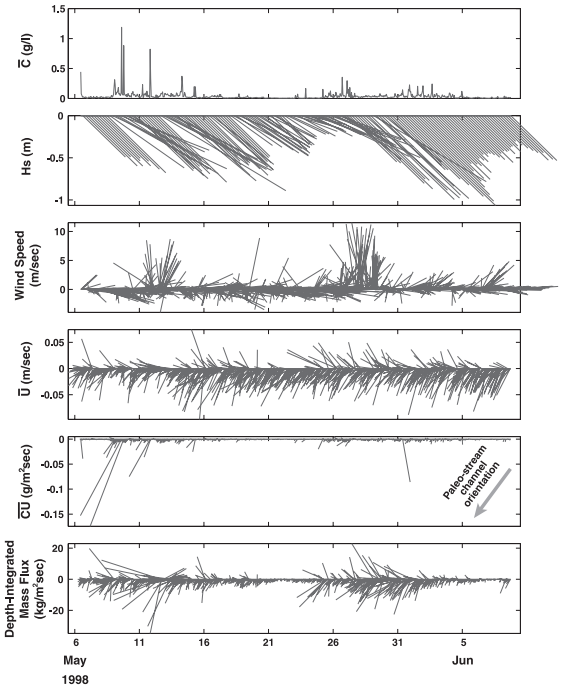

Fig. 12. Time series of burst-averaged suspended-sediment concentration, wave height and direction, wind speed and direction, mean current speed and direction, the resulting magnitude and direction of suspended-sediment transport at the elevation of the EMCM and OBS, and the modeled depth-integrated suspended-sediment mass flux magnitude and direction. Note that although the wind and waves typically come out of the west to northwest, the mean current and thus the direction of sediment transport and mass flux are primarily directed offshore and thus appear to be controlled by the orientation of the sediment-filled paleo-stream channel. All vectors are projected geographically (north = up, east = right).

direction of the wind and the waves (Fig. 12). We emphasize that this southwest direction is oriented offshore along the axis of the sediment-filled paleo-stream channel. It appears that the wave- (and likely wind-) driven onshore transport in the upper portion of the water column is balanced by downwelling benthic mean flows, similar to the near-bed offshore currents observed by Wright et al. (1986, 1991) during storms. In our case, however, the flow appears to be constrained by the incised paleo-stream channel. The mean orientation of the currents is parallel to the trend of the channel and the variation of current direction is small. Since the direction of near-bed suspended-sediment transport and the depth-integrated mass flux are controlled by the direction of the mean current, they, too, are primarily directed offshore through the paleo-stream channel. This pattern is different from the wind-driven flow and resulting sediment transport observed along relatively linear, sandy shorelines (Vincent et al., 1983; Madsen et al., 1993), but it is similar to that observed by Field and Roy (1984) off the rocky shoreline of Australia.

Of note is the difference between the suspended-sediment transport observed at the elevation of the sensors ($F_{obs} = \overline{UCg}$) and the mass flux calculated by the Madsen (1994) model (F_{mod}) for the same elevation (Fig. 13). Not only does the model underestimate the magnitude of suspended-sediment flux, but it also cannot match the timing of periods of high suspended-sediment flux. This reflects the development of the model for the conditions on the mid- and outer shelf where the magnitude of wind-driven flows are on the scale of the orbital wave motions (Sherwood et al., 1994; Ogston and Sternberg, 1999; Wright et al., 1999). In the Madsen (1994) model, sediment flux is calculated by the product of the mean suspended-sediment concentration with the mean current velocity. In contrast, in the shallow depths of the inner shelf, waves dominate the near-bed flow and therefore the stress on the bed, and sediment suspension is tightly tied to the passage of

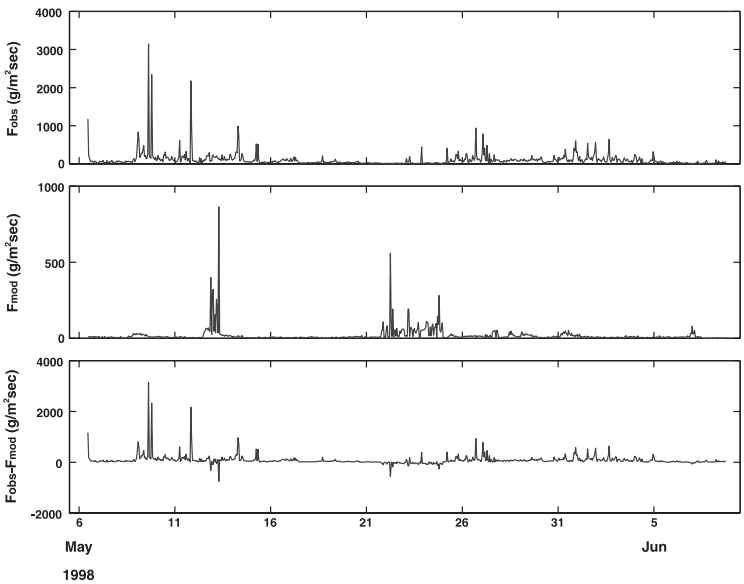

Fig. 13. Comparison of the observed suspended-sediment mass flux (F_{obs}) at the level of the EMCM and OBS sensors versus the mass flux at the level of the sensors computed by the Madsen (1994) model (F_{mod}). Not only does the model underestimate the magnitude of suspended-sediment mass flux, but it also cannot match the timing of periods of high mass flux. This is due to the model's use of the mean suspended-sediment concentration and the mean current velocity and not the instantaneous coupling between flow and sediment suspension.

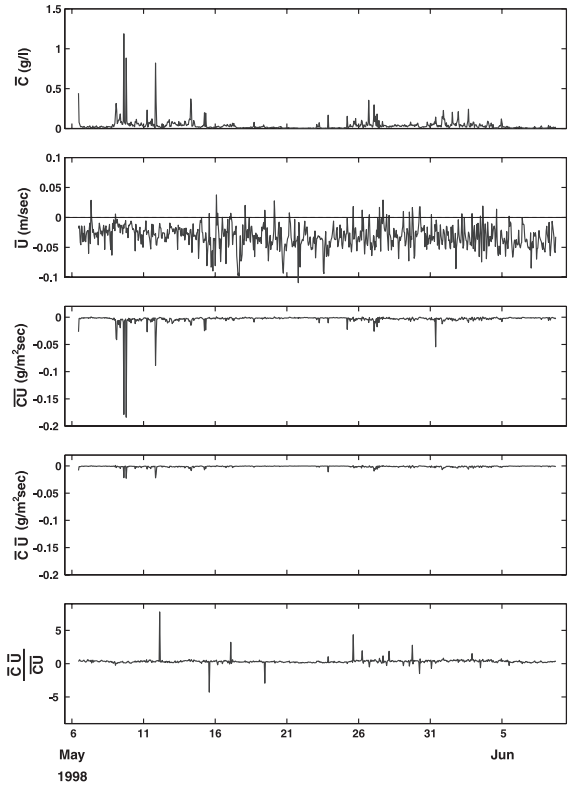

Fig. 14. Burst-averaged mean concentration, mean current, the resulting suspended-sediment transport calculated using the product of the mean current velocity and the mean suspended-sediment concentration ($\overline{UC}$), and the resulting suspended-sediment transport using the mean of the product of the instantaneous current velocity and the instantaneous suspended-sediment concentration ($\overline{UC}$), which takes into account 'flux coupling' (Jaffe et al., 1985) or the instantaneous coupling of flow and sediment suspension. Note that by not incorporating the 'flux coupling', both the magnitude and direction of suspended-sediment flux will be evaluated.

individual waves and the interactions between wave groups. Jaffe et al. (1985) demonstrated the importance of this 'flux coupling', or the instantaneous coupling between flow and sediment suspension in the surf zone where wave motions dominate the near-bed flow. In Fig. 14 we show that calculating the suspended-sediment flux using actual observations from the OBS and EMCM sensors can produce widely different results by incorporating the instantaneous coupling between flow and sediment ($\overline{UC}$) versus using the burst-averaged product of the flow and suspended-sediment concentration ($\overline{UC}$). Since the present models of sediment transport on the shelf do not use the instantaneous coupling of flow and sediment, they will inevitably under-predict the magnitude and incorrectly predict the direction of suspended-sediment transport. New, time-dependent models must be used in order to model suspended-sediment transport accurately on the inner shelf where wave motions dominate over mean currents.

The observations and modeling have implications for the distribution of sediment on the shelf. Both the observed and modeled suspended-sediment transport is oriented primarily offshore at the study site. One would infer that this means the location of the instrument is a conduit for sediment to be transported from the inner shelf to the mid- and outer shelf. When reflecting on the temporal structure of the SSEs, however, it seems likely that a number of grain sizes with different settling velocities were advected past the OBS sensor during the course of the deployment. If this is the case, we may be observing a partitioning of the sediment during onshore SSEs that contributes to the development of the two primary sedimentary provinces observed by Edwards (2002): an inshore littoral sand belt and a mid-shelf mud belt. During the initial increase in concentration when the flow is directed onshore, larger (sand-sized) particles are carried onshore and fall out of suspension before the near-bed flow reverses. Particles still in suspension after the first 1–2 s of the SSE are probably smaller, and these smaller particles are transported offshore during the latter part of the onshore event. Mid-shelf mud belts, common on many shelves including central California, may receive a portion of their sediment through this process.

5. Conclusions

Sediment suspension on a rocky, high-energy inner shelf is often very episodic. During the deployment, 9567 SSEs were observed. The events were strongly correlated to incident waves and wave groups, which were shown to dominate the near-bed flow at the study site. On average, the

events that started under onshore flow were of longer duration than those that began during offshore flow. The longer duration of the events that started during onshore flow caused a net offshore flux of sediment due to a flow reversal before the sediment settled out. Although sediment suspension appears to be primarily controlled by wave orbital motions, the direction of net suspended-sediment transport for all events, which is driven by the orientation of the mean currents, was primarily offshore, oriented along the axis of the paleo-stream channel. These downwelling benthic mean flows appear to balance strong wind- and wave-driven onshore transport during storms. Assuming the phenomena observed were typical for a paleo-stream channel flanked by bedrock highs, we must conclude that the direction of mean flow and the resulting sediment transport is largely a function of the inner shelf morphology and is primarily directed offshore during high-energy events. The initial results discussed here have simply identified the nature of the near-bed flow regime and sediment suspension on a high-energy, rocky shoreface. Much more data are needed from the central coast of California and other rocky shorefaces before any generalizations regarding the nature of hydrodynamics and sediment transport in such an environment can be drawn. Only by expanding our sparse database on the mechanisms that drive sediment fluxes under varying energy conditions and over different rocky shoreface configurations, will we gain better insight into the linkages between the surf zone and the shelf.

Acknowledgements

This research was made possible through funding from the US Geological Survey's Western Coastal and Marine Geology Program's Monterey Bay National Marine Sanctuary Project directed by Steve Eittreim and the US Geological Survey's Western Coastal and Marine Geology Program-University of California, Santa Cruz's Coastal Geology and Imaging Laboratory Co-operative (USGS/CMG-UCSC/CGIL Co-Op). We would like to extend sincere thanks to Gary Griggs (UCSC) and Roberto Anima (USGS) for their insight, cooperation, and friendship that contributed substantially to the goals of this project. Chris Sherwood (USGS) provided the Madsen (1994) spectral wave–current bottom boundary layer model, Joanne Thede Ferreira (USGS) developed the SHAST logging software, and Dave Gonzales (USGS) provided the much-needed sensor and instrumentation support. Tom Reiss (USGS) and Rob Britts (USGS) provided invaluable help leading the bathymetric survey. Don Canestro (UCSC) and Pete Dal Ferro (UCSC) led the instrument deployment and recovery efforts both as divers and boat operators; more importantly, they kept CDS alive underwater under some nasty conditions. Robert Anderson (UCSC), Michael Field (USGS), and Jingping Xu (USGS) provided an initial review of the manuscript and offered thoughtful and helpful suggestions. We would also like to thank the two anonymous reviewers and Marlene Noble (USGS) for their editing and technical review of this manuscript.

References

Anima, R.J., 2000. Nearshore and Continental Shelf Morphology, Paleomorphology, Sediment Transport based on High-Resolution Geophysical Profiling of the Monterey Bay National Marine Sanctuary. Ph.D. Thesis. University of California at Santa Cruz, Santa Cruz, CA.

Birkemeier, W.A., Baron, C.F., Leffler, M.W., Hathaway, K.K., Miller H.C., Strider, J.B., 1989. SUPERDUCK Nearshore Processes Experiment Data Summary: CERC Field Research Facility. US Army Corps of Engineers Miscellaneous Paper CERC-89-16.

Cacchione, D.A., Drake, D.E., 1982. Measurements of storm-generated bottom stress on the continental shelf. J. Geophys. Res. 87, 1952–1960.

Cacchione, D.A., Drake, D.E., Grant, W.D., Tate, G.B., 1984. Rippled scour depressions on the inner continental shelf off central California. J. Sediment. Petrol. 54, 1280–1291.

Cacchione, D.A., Field, M.E., Drake, D.E., Tate, G.B., 1987. Crescentic dunes on the inner continental shelf off northern California. Geology 15, 1134–1137.

Csanady, G.T., 1982. Gradation in the Coastal Ocean. Reidel, Dordrecht.

Dick, J.E., Erdman, M.R., Hanes, D.M., 1994. Suspended sand concentration events due to shoaled waves over a flat bed. Mar. Geol. 119, 67–73.

Edwards, B.D., 2002. Surface sediment characteristics of the MBNMS continental shelf. Mar. Geol. 181, 195–213.

Field, M.E., Roy, P.S., 1984. Offshore transport and sandbody formation: evidence from a steep high-energy shoreface southeastern Australia. J. Sediment. Petrol. 54, 1292–1302.

Foreman, M.G.G., Henry, R.F. 1979. Tidal Analysis based on High and Low Water Observations. Pacific Marine Science Report 79-15. Institute of Ocean Sciences, Patricia Bay, Sidney, BC.

Foster, D.L., 1997. Dynamics of the Nearshore Wave Bottom Boundary Layer. Ph.D. Thesis. Oregon State University, Corvallis, OR.

Gallagher, E.L., Boyd, W., Elgar, S., Guza, R.T., Woodward, B., 1996. Performance of a sonar altimeter in the nearshore. Mar. Geol. 133, 241–248.

Hanes, D.M., 1991. Suspension of sand due to wave groups. J. Geophys. Res. 96, 8911–8915.

Hanes, D.M., Huntley, D.A., 1986. Continuous measurements of suspended sand concentration in a wave dominated nearshore environment. Cont. Shelf Res. 6, 585–596.

Hay, A.E., Bowen, A.J., 1994. Coherence of wave-induced suspended sand concentration fluctuations. J. Geophys. Res. 99, 12749–12765.

Huntley, D.A., Hanes, D.M., 1987. Direct measurement of suspended sediment transport. In: Coastal Sediments '87, vol. 1. American Society of Civil Engineers, pp. 723–733.

Jaffe, B.E., Sternberg, R.W., Sallenger, A.H., 1985. The role of suspended sediment in shore-normal beach profile changes. In: Proceedings of the 19th Coastal Engineering Conference, vol. 2. American Society of Civil Engineers, pp. 1983–1996.

Jaffe, B.E., Sallenger, A., 1992. The contribution of suspension events to sediment transport in the surf zone. In: Proceedings of the 23rd Coastal Engineering Conference, vol. 3. American Society of Civil Engineers, pp. 2680–2693.

List, J.H., 1991. Wave groupiness variations in the nearshore. Coast. Eng. 15, 475–496.

Madsen, O.S., 1994. Spectral wave–current bottom boundary layer flows. In: Proceedings of the 24th Coastal Engineering Conference, vol. 1. American Society of Civil Engineers, pp. 384–398.

Madsen, O.S., Wright, L.D., Boon, J.D., Chisholm, T.A., 1993. Wind stress bed roughness and sediment transport on the inner shelf during an extreme storm event. Cont. Shelf Res. 13, 1303–1324.

Meteorology International, 1977. Deep-water Wave Statistics for the California Coast. Prepared for the Department of Navigation and Ocean Development, Sacramento, CA.

National Marine Consultants, 1960. Wave Statistics for Seven Deep Water Stations along the California Coast. Report prepared for the US Army Corps of Engineers, Los Angeles and San Francisco Districts, CA.

Niedoroda, A.W., Swift, D.J.P., Hopkins, T.S., Ma, C.-M., 1984. Shoreface morphodynamics on wave-dominated coasts. Mar. Geol. 60, 331–354.

Ogston, A.S., Sternberg, R.W., 1999. Sediment-transport events on the northern California continental shelf. Mar. Geol. 154, 69–82.

Osborne, P.D., Greenwood, B., 1992. Frequency dependent cross-shore suspended sediment transport 2. A barred shoreface. Mar. Geol. 106, 25–51.

Page, B.M., Thompson, G.A., Williams, R.G., 1998. Late Cenezoic tectonics of the central and southern Coastal Ranges of California. GSA Bull. 110, 846–876.

Seymour, R.J., 1986. Nearshore autosuspending turbidity currents. Ocean Eng. 13, 435–447.

Sherwood, C.R., Butman, B., Cacchione, D.A., Drake, D.E., Gross, T.F., Sternberg, R.W., Wiberg, P.L., Williams, A.J., 1994. Sediment-transport events on the northern California continental shelf during the 1990–1991 STRESS experiment. Cont. Shelf Res. 14, 1063–1099.

Shi, N.C., Larsen, L.H., 1984. Reverse sediment transport induced by amplitude modulated waves. Mar. Geol. 54, 181–200.

Signell, R.P., Jenter, H.L., Blumberg, A.F., 1996. Circulation and Effluent Dilution Modeling in Massachusetts Bay: Model Implementation, Verification and Results. US Geological Survey Open-file Report 96-015.

Signell, R.P., 1989. Tidal Dynamics and Dispersion around Coastal Headlands. Ph.D. Thesis. Massachusetts Institute of Technology, Woods Hole Oceanographic Institution, Cambridge, MA.

Storlazzi, C.D., 2000. Hydrodynamics, Sediment Transport, and El Niño-induced Seacliff Erosion along the Coastline of Central California. Ph.D. Thesis. University of California at Santa Cruz, Santa Cruz, CA.

Storlazzi, C.D., Field, M.E., 2000. Sediment distribution and transport along a rocky embayed coast: Monterey Peninsula and Carmel Bay California. Mar. Geol. 170, 289–316.

Strub, P.T., Allen, J.S., Huyer, A., Smith, L., Beardsley, R.C., 1987. Seasonal cycles of currents temperature, winds, and sea leverl over the northeast Pacific continental shelf: 35°N to 48°N. J. Geophys. Res. 92, 1507–1526.

Tait, J.F., 1995. Rocky Coasts and Inverse Methods: Sediment Transport and Sedimentation Patterns of Monterey Bay National Marine Sanctuary. Ph.D. Thesis. University of California at Santa Cruz, Santa Cruz, CA.

Tait, J.F., Anima, R.J., Griggs, G.B., 1992. Shoreface storage and transport of littoral sediments along the central California coast (abstract). EOS Trans. Am. Geophys. Union 73.

US Army Corps of Engineers, 1985. Geomorphology Framework Report: Monterey Bay, Los Angeles, CA. Coast of California Storm and Tidal Waves Study Report CCSTWS 85-2.

Vincent, C.E., Young, R.A., Swift, D.J.P., 1983. Sediment transport on the Long Island shoreface North American Atlantic Shelf: role of waves and currents in shoreface maintenance. Cont. Shelf Res. 2, 163–181.

Vincent, C.E., Hanes, D.M., Bowen, A.J., 1991. Acoustic measurements of suspended sand on the shoreface and the control of concentration by bed roughness. Mar. Geol. 96, 1–18.

Wright, L.D., 1987. Shelf-surfzone coupling: diabathic shoreface transport. In: Coastal Sediments '87, vol. 1. American Society of Civil Engineers, pp. 25–40.

Wright, L.D., Boon, J.D., Green, M.O., List, J.H., 1986. Response of the mid shoreface of the southern Mid-Atlantic Bight to a 'Northeaster'. Geol.-Mar. Lett. 6, 153–160.

Wright, L.D., Boon, J.D., Kim, S.-C., List, J.H., 1991. Modes of cross-shore sediment transport on the shoreface of the Middle Atlantic Bight. Mar. Geol. 96, 19–51.

Wright, L.D., Kim, S.-C., Friedrichs, C.T., 1999. Across-shelf variations in bed roughness bed stress, and sediment suspension on the northern California shelf. Mar. Geol. 154, 99–115.

Xu, J.P., Noble, M., Eittreim, S.L., 2001. Suspended sediment transport on the continental shelf near Davenport. California. Mar. Geol. 181, 171–193.